Journal of
Micro/Nanolithography,
MEMS, and MOEMS

Nanolithography.SPIEDigitalLibrary.org

Emulation of anamorphic imaging on the SHARP extreme ultraviolet mask microscope

Markus P. Benk
Antoine Wojdyla
Weilun Chao
Farhad Salmassi
Sharon Oh
Yow-Gwo Wang
Ryan H. Miyakawa
Patrick P. Naulleau
Kenneth A. Goldberg

SPIE.

Markus P. Benk, Antoine Wojdyla, Weilun Chao, Farhad Salmassi, Sharon Oh, Yow-Gwo Wang, Ryan H. Miyakawa, Patrick P. Naulleau, Kenneth A. Goldberg, "Emulation of anamorphic imaging on the SHARP extreme ultraviolet mask microscope," *J. Micro/Nanolith. MEMS MOEMS* **15**(3), 033501 (2016), doi: 10.1117/1.JMM.15.3.033501.

Downloaded From: http://nanolithography.spiedigitallibrary.org/ on 07/15/2016 Terms of Use: http://spiedigitallibrary.org/ss/TermsOfUse.aspx

Emulation of anamorphic imaging on the SHARP extreme ultraviolet mask microscope

Markus P. Benk,* Antoine Wojdyla, Weilun Chao, Farhad Salmassi, Sharon Oh, Yow-Gwo Wang, Ryan H. Miyakawa, Patrick P. Naulleau, and Kenneth A. Goldberg
Center for X-ray Optics, Lawrence Berkeley National Laboratory, 1 Cyclotron Road, Berkeley, California 94720, United States

Abstract. The SHARP high-numerical aperture actinic reticle review project is a synchrotron-based, extreme ultraviolet (EUV) microscope dedicated to photomask research. SHARP emulates the illumination and imaging conditions of current EUV lithography scanners and those several generations into the future. An anamorphic imaging optic with increased mask-side numerical aperture (NA) in the horizontal and increased demagnification in the vertical direction has been proposed to overcome limitations of current multilayer coatings and extend EUV lithography beyond 0.33 NA. Zoneplate lenses with an anamorphic $4\times/8\times$ NA of 0.55 are fabricated and installed in the SHARP microscope to emulate anamorphic imaging. SHARP's Fourier synthesis illuminator with a range of angles exceeding the collected solid angle of the newly designed elliptical zoneplates can produce arbitrary angular source spectra matched to anamorphic imaging. A target with anamorphic dense features down to 50-nm critical dimension is fabricated using 40 nm of nickel as the absorber. In a demonstration experiment, anamorphic imaging at 0.55 $4\times/8\times$ NA and 6 deg central ray angle (CRA) is compared with conventional imaging at 0.5 $4\times$ NA and 8 deg CRA. A significant contrast loss in horizontal features is observed in the conventional images. The anamorphic images show the same image quality in the horizontal and vertical directions. © *2016 Society of Photo-Optical Instrumentation Engineers (SPIE)* [DOI: 10.1117/1.JMM.15.3.033501]

Keywords: extreme ultraviolet; anamorphic; mask; microscope; zone plate; high-numerical aperture.

Paper 16039P received Apr. 6, 2016; accepted for publication Jun. 20, 2016; published online Jul. 12, 2016.

1 Introduction

The insertion of extreme ultraviolet lithography (EUVL) into production is likely to happen at the 7-nm logic node, corresponding to k_1 factors well below 0.5 at 0.33 NA.[1] Feature sizes at these nodes require the use of resolution enhancement techniques in EUVL from the start, not leaving much room to further decrease critical dimensions (CD) without using double patterning.[2] The next generation of EUVL at higher NA is under development now and will be required soon after the insertion of EUVL into production in order to keep the technology on track down to smaller feature sizes.

The wafer-side NA of a lithography system may be increased by either increasing the mask-side NA, increasing the demagnification of the system, or a combination of the two. An increased mask-side NA creates an increased angular extent of the incoming and outgoing light cones. Separating the cones requires an increased central ray angle (CRA) at the photomask to avoid overlap.[3] In the plane of incidence, the increased range of angles on the photomask, offset by an increased CRA, exceeds the angular bandwidth of current multilayer reflective coatings, thus reducing image contrast. Perpendicular to the plane of incidence, the range of angles does not exceed the bandwidth of the multilayer coating. For horizontal features, perpendicular to the plane of incidence, the illumination is offset by the central ray angle, and shadowing from the thick absorber can degrade imaging performance. For vertical features, parallel to the plane of incidence, the illumination is centered, causing less shadowing.

EUV projection lenses at higher demagnification ratios beyond 4× show acceptable imaging performance. However, printing one full field at two times higher demagnification either requires a photomask with four times the surface area, or the field needs to be stitched from four quarter-field exposures. Neither of these options is considered economically viable.[4]

Zeiss and ASML have proposed an anamorphic projection optic with increased mask-side NA perpendicular to the plane of incidence and increased demagnification in the plane of incidence.[5] Such a design avoids high angles of incidence on the photomask in the plane of incidence (that would degrade image quality) while preserving the demagnification perpendicular to the plane of incidence. This allows stitching one full field on the wafer from two half-field exposures instead of four quarter fields. The angular bandwidth of the multilayer is most efficiently used. An anamorphic projection optic with a wafer-side NA of 0.55 is discussed in Ref. 6.

Aerial mask imaging tools are currently used in EUV research and process development and will be required for EUV production. SHARP is a synchrotron-based, actinic, EUV mask microscope located at a bending-magnet beamline at the Advanced Light Source at Lawrence Berkeley National Laboratory. Since its commissioning in 2013, SHARP has contributed to many aspects of EUV mask technology, including defects,[7] their detection[8] and printability,[9] repairs,[10] substrate roughness,[10] impact of nontelecentricity,[11] and multilayer properties.[12] An overview of SHARP can be found in Ref. 13.

*Address all correspondence to: Markus P. Benk, E-mail: mpbenk@lbl.gov

1932-5150/2016/$25.00 © 2016 SPIE

Downloaded From: http://nanolithography.spiedigitallibrary.org/ on 07/15/2016 Terms of Use: http://spiedigitallibrary.org/ss/TermsOfUse.aspx

SHARP is designed to emulate imaging in EUV scanners. The tool records a series of aerial images of a feature or defect on the photomask, matching the mask-side NA of the scanner and emulating the angular spectrum of the illumination, including the chief-ray angle and azimuthal rotation of the plane of incidence across the field. The SHARP aerial image is therefore similar to the wafer print, allowing the user to assess the characteristics of a feature or defect with respect to printing on a wafer. Figure 1 shows a comparison of (a) a mask-scanning electron microscopic (SEM) image, (b) SHARP aerial image, and (c) wafer-SEM. The images are taken from Ref. 14. The SHARP aerial image closely matches the wafer print. The mask-SEM shows the defect but does not reveal the extent of the damage to the multilayer surrounding the visible defect.

SHARP uses a wide range of off-axis Fresnel zoneplate lenses as imaging optics, matching the mask-side NA of current and future generations of EUVL, including the ASML ADT and NXE 3100 to 3500 scanners. The tool's standard zoneplates range from 0.25 4× NA up to 0.625 4× NA. A resolution of 22 nm half-pitch (hp) on the mask side, corresponding to 5.5 nm hp on the wafer side in a 4× lithography system, has been demonstrated for the 0.625 4× NA lens.[15] To emulate the source angular spectrum of the scanner, SHARP has a fully programmable Fourier synthesis illuminator.[16]

SHARP's flexible design allows it to respond to new developments in EUVL and to emulate arbitrary technologies under consideration. This enables research many years into the future of EUV lithography. Recently, SHARP has been upgraded to emulate anamorphic imaging, providing a platform for research in this emerging area.

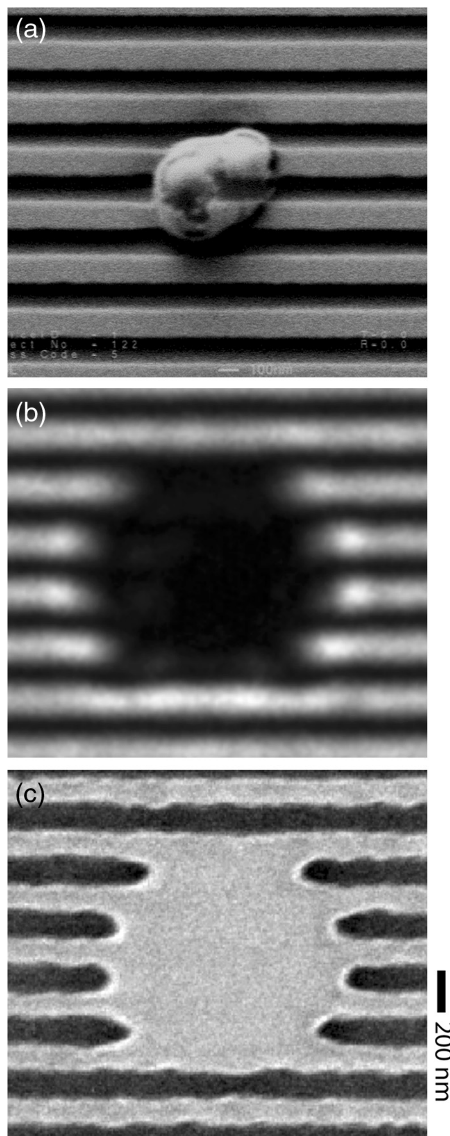

Fig. 1 Visual comparison of a large defect,[13] imaged with (a) mask-SEM, (b) SHARP EUV mask microscope, and (c) wafer-SEM.

2 Emulation of Anamorphic Imaging

SHARP emulates the source angular spectrum and mask-side NA values; emulating anamorphic imaging requires the corresponding illuminator and elliptical mask-side illumination solid angle. Since SHARP's Fourier synthesis illuminator can reach angles of incidence up to 19 deg off-axis at the mask (well beyond typical multilayer angular bandpass limits), all anamorphic imaging configurations can be generated. Figure 2 shows a pixelated cross pole illuminator rendered

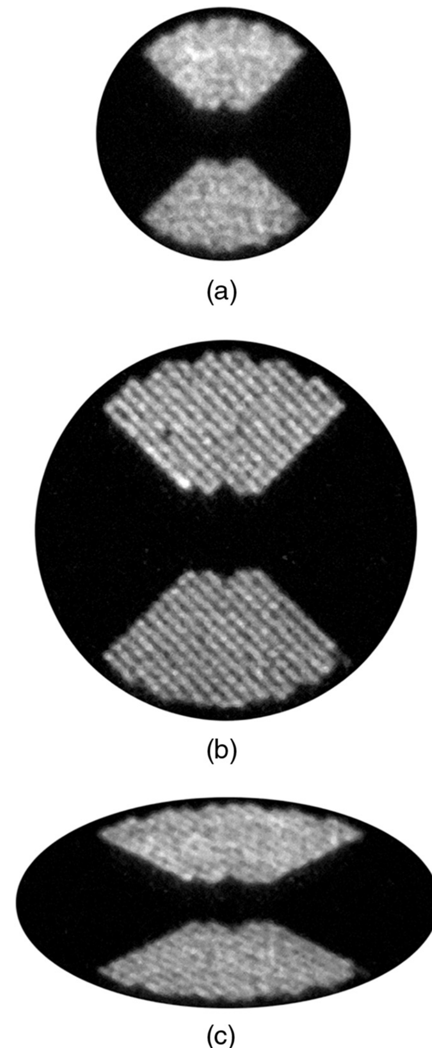

Fig. 2 Pixelated cross pole illuminator, matched to (a) the 0.33 4× NA lens at 6 deg CRA, (b) 0.5 4× NA lens at 8 deg CRA, and (c) anamorphic imaging at 0.55 4×/8× NA and 6 deg CRA in comparison, recorded with a YAG scintillator camera in SHARP microscope.

Downloaded From: http://nanolithography.spiedigitallibrary.org/ on 07/15/2016 Terms of Use: http://spiedigitallibrary.org/ss/TermsOfUse.aspx

for (a) the 0.334× NA lens at 6 deg CRA, (b) 0.5 4× NA lens at 8 deg CRA, and (c) anamorphic imaging at 0.55 4 × /8× NA and 6 deg CRA in comparison. The images are recorded with a YAG scintillator camera, installed in the tool for monitoring the source angular spectrum. The individual pupil channels (pixels) can be seen in the high-NA pupils. For 0.33 4× NA, the angular divergence of the synchrotron beam matches the solid angle of the pupil channels, making them indistinguishable.

2.1 *Zoneplate*

Figure 3 shows the apertures (gray) of (a) a 0.33 4× NA zoneplate at 6 deg CRA, (b) a 0.5 4× NA zoneplate at 8 deg CRA, and (c) a 0.55 4 × /8× NA zoneplate for anamorphic imaging at 6 deg CRA in comparison. The difference in the angular range with respect to the normal ray on the photomask can be seen. Figure 4 shows the calculated reflectivity of a typical Mo/Si multilayer on a photomask at 13.5-nm wavelength as a function of the angle of incidence. The reflectivity curve is almost flat from normal incidence to about 11 deg from normal, then starts rolling off toward larger angles. The end of the useable angular bandwidth at 11 deg is marked in Figs. 3 and 4.

The aperture of a zoneplate for anamorphic imaging is defined by the intersection of the elliptic cone of a given NA with a plane, tilted by the CRA (6 deg). The normal distance from the tip of the cone to the intersecting plane sets the working distance of the zoneplate. The mask-side coherent resolution of the lens $r_c = 0.5\lambda/\text{NA}$ is approximately 45.5-nm hp in the lateral, high-NA (4×) orientation, which is the x-direction in the image, and is approximately 91-nm HP in the low-NA (8×) orientation, which is the y-direction in the image. The mask-side resolution limits are calculated using the mask-side NA values in the equation. The zoneplate as a single optical element does not provide anamorphic imaging, i.e., different magnifications in the x- and y-direction. Collecting the proper solid angle, however, captures the characteristics of the anamorphic image, and the aspect ratio can easily be corrected, scaling the digital image in one dimension.

The 0.55 4 × /8× NA zoneplate is fabricated in three different working distances: 360, 320, and 275 μm, with approximate magnifications of 1250×, 1400×, and 1640×. The lowest magnification corresponds to 5 pixels per resolution element in the high-NA (4×) orientation. In the low-NA (8×) orientation, there are twice as many pixels per resolution element in the raw image. After scaling the image by a factor of two, the number of pixels per resolution element consequently matches in the x- and y-directions. The lowest-magnification lens produces the brightest picture and offers the largest working distance. For experiments where higher sampling is desired, the highest magnification, with 6.5 pixels per resolution element, can be used.

Like SHARP's standard zoneplates, the 0.55 4 × /8× NA zoneplates are patterned with e-beam lithography and electroplated using 35 nm of gold on a 100-nm silicon nitride membrane. The SEM images in Fig. 5 show one of the anamorphic zoneplates (a) and a detail of its outer zones (b). The zone pattern is not resolved in Fig. 5(a), causing a moiré pattern.

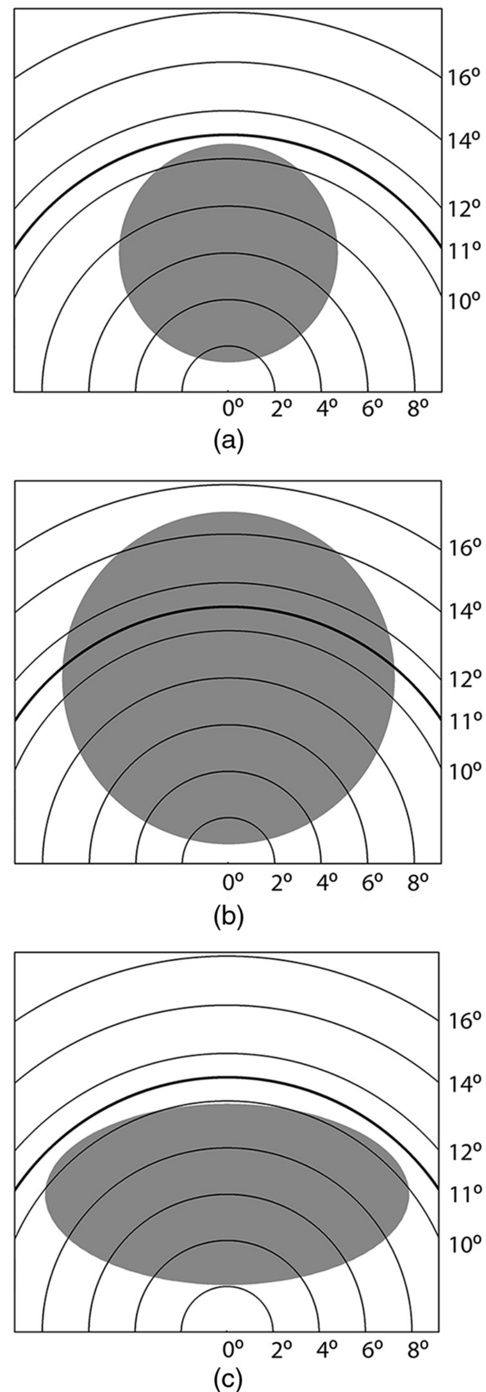

Fig. 3 Apertures of: (a) a 0.33 4× NA zoneplate at 6 deg CRA, (b) 0.5 4× NA zoneplate at 8 deg CRA, and (c) 0.55 4 × /8× NA zoneplate for anamorphic imaging at 6 deg CRA in comparison and range of angles of the associated ray cones.

2.2 *Target Fabrication*

In order to demonstrate anamorphic imaging on the SHARP microscope, a set of anamorphic test patterns is fabricated. Three different aspect ratios of the patterns are realized. The ratios are standard 4×, 4 × /8× for the anamorphic imaging demonstration, and 4.8 × /7.5×. This latter aspect ratio is discussed in Ref. 5. Just like 4 × /8×, it allows for stitching one full field from two half fields using a slightly wider and shorter region of the photomask and collecting a slightly

Downloaded From: http://nanolithography.spiedigitallibrary.org/ on 07/15/2016 Terms of Use: http://spiedigitallibrary.org/ss/TermsOfUse.aspx

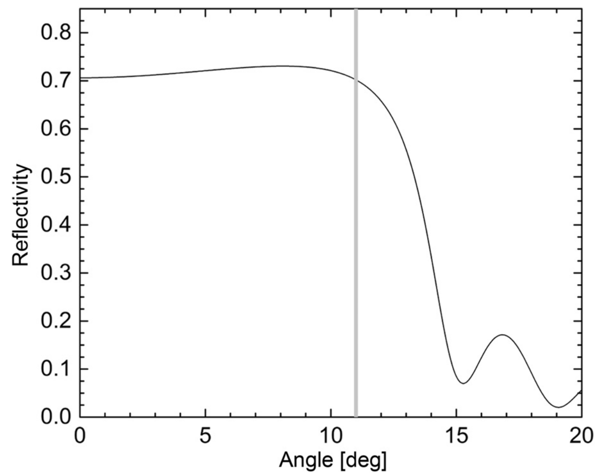

Fig. 4 Calculated reflectivity of a typical multilayer coating on an EUV photomask at 13.5-nm wavelength as a function of the angle of incidence.

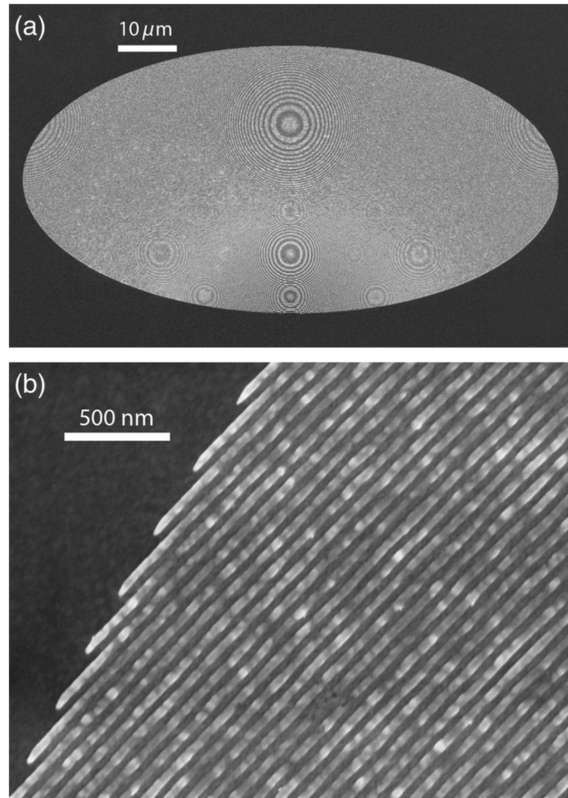

Fig. 5 SEM-image of: (a) a zoneplate lens with an anamorphic aperture and (b) detail image, showing the outer zones.

different solid angle from the mask. Zoneplates for this aspect ratio will be included in the next production run.

Aiming at a short production time, the target is patterned in-house at the CXRO nanofabrication laboratory on a silicon wafer in a nickel lift-off process instead of using an EUV photomask blank with a tantalum-based absorber. The wafer is coated with a standard Mo/Si multilayer and ruthenium capping layer. The wafer is then coated with polymethylmethacrylate (PMMA) and patterned using electron-beam lithography. After development, a 2-nm assist layer of chrome is deposited for adhesion, and 40 nm of nickel are deposited as the absorber.

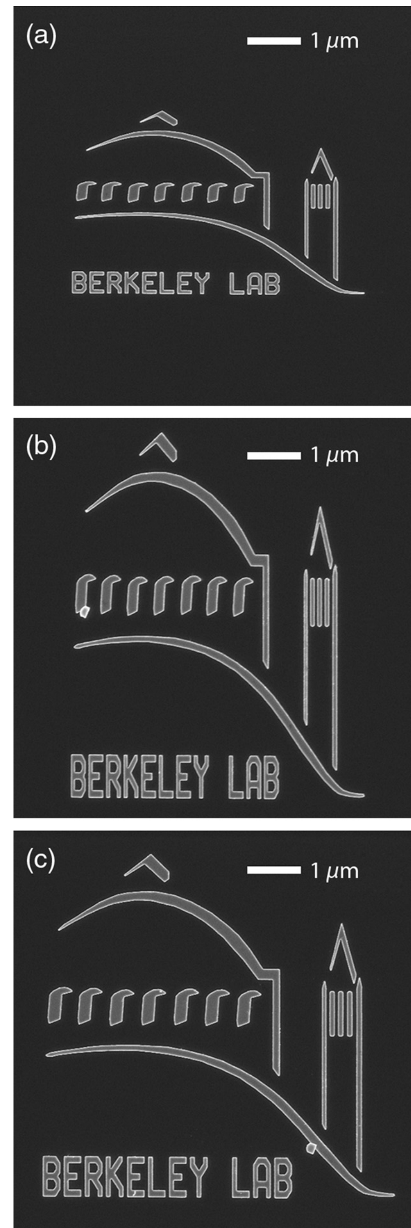

Fig. 6 SEM-images of (a) 4× reference pattern, (b) anamorphic $4\times/8\times$, and (c) $7.5\times/4.8\times$ test patterns.

Chrome and nickel adhere to the clear multilayer. The chrome and nickel on the resist are lifted off together with the resist material in an etch step, leaving nickel patterns. The wafer is then mounted on a mask substrate for loading into SHARP. The target has patterns down to 50-nm CD. Figure 6 shows three SEM images of the LBNL logo that is part of the test patterns. (a) The conventional 4×, (b) $4\times/8$, and (c) $4.8/7.5\times$ aspect ratios are shown side by side.

3 Imaging Results

Different test patterns are imaged using Quasar-45 illumination with a 45-deg arc angle, an inner σ of 0.2, and an outer σ of 0.9. The parameter σ, ranging from zero to one, describes the angular extension of the illumination relative to the NA of the imaging optic. Figure 7(a) shows a SHARP image of a test pattern with 50-nm CD (mask scale), recorded with the

Downloaded From: http://nanolithography.spiedigitallibrary.org/ on 07/15/2016 Terms of Use: http://spiedigitallibrary.org/ss/TermsOfUse.aspx

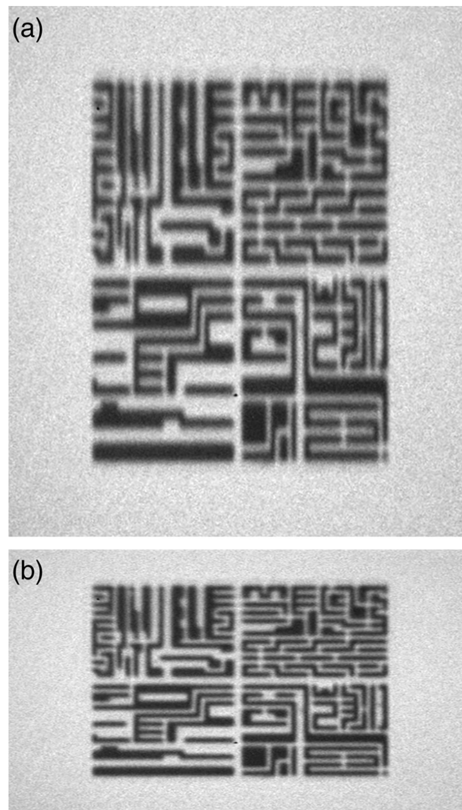

Fig. 7 (a) SHARP image of anamorphic test pattern with 50-nm CD (mask scale) and (b) scaled version of the image with corrected magnifications in the x- and y-directions. The image is recorded at a magnification of 1250× using Quasar-45 illumination with a 45-deg arc angle, an inner σ of 0.2, and an outer σ of 0.9. The effective magnification in (b) the scaled image is reduced to 625 in the y-direction. The magnification in the x-direction remains 1250×.

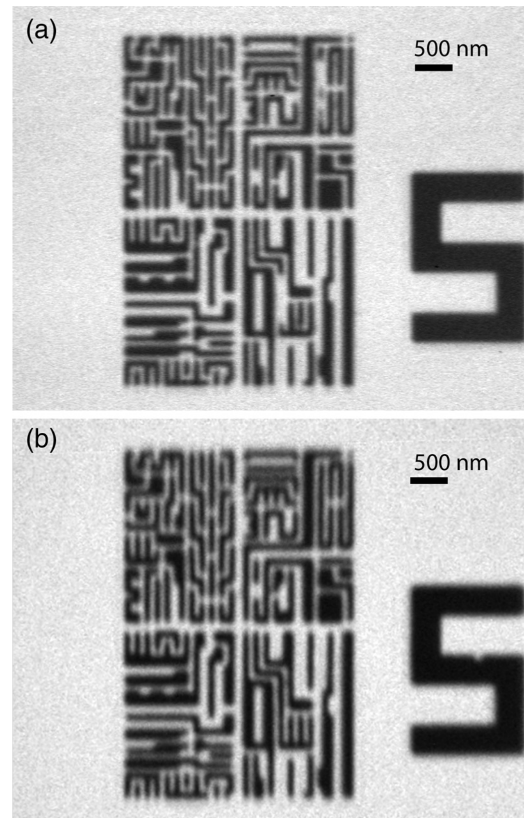

Fig. 8 SHARP aerial images of a test pattern with 50-nm CD (mask scale), comparing (a) anamorphic imaging at 0.55 4 × /8× NA (6 deg CRA) with (b) conventional (isomorphic) imaging at 0.5 4× NA (8 deg CRA).

0.55 4 × /8× NA lens. Figure 7(b) shows the same image scaled to match the difference in magnification in x and y in the anamorphic image. The scaled image shows the pattern as it is intended on the wafer. Scaling of the image is shown here in an example. Further anamorphic images shown in this paper are already scaled and interpolated to a finer grid.

Images of a test pattern with 50-nm CD (mask scale) are shown in Fig. 8, comparing (a) anamorphic imaging at 0.55 4 × /8× NA (6 deg CRA) with (b) conventional (isomorphic) imaging at 0.5 4× NA (8 deg CRA). In the anamorphic image, the pattern is resolved, showing the same image quality on horizontal and vertical features. In the conventional image, vertical features are resolved, but the image contrast is reduced on horizontal features. This is due to the angular range of the collected solid angle exceeding the angular bandwidth of the multilayer and due to vertical shadowing from absorber features, as discussed in Sec. 1.

Fifty-nm CD elbows (mask scale) are shown in Fig. 9, again comparing (a) anamorphic imaging at 0.55 4 × /8× NA (6 deg CRA) with (b) conventional (isomorphic) imaging at 0.5 4× NA (8 deg CRA). As in the previous example, the anamorphic image shows the same image quality in the x- and y-directions. In the conventional image, only vertical features are resolved. The high angles of incidence and shadowing from the absorber lead to loss of contrast on horizontal features. Figure 9(c) shows an SEM image of the 4× elbow on the target. The SEM shows some small pattern defects that can be seen in the SHARP image as well. The pattern quality on the mask is equal in the horizontal and vertical directions; thus, the imaging nonuniformity seen in SHARP is wholly attributable to image formation at wavelength.

Cross-section plots through the horizontal and vertical features in the elbows from Fig. 9 are shown in Fig. 10. The cross-sections are averaged over 30 pixels, parallel to the line directions. The profiles are normalized by defining the intensity of the clear region around the elbow to be one. The horizontal and vertical line profiles from (a) the anamorphic image are similar, with a modulation of 44%. The cross-section plot of the vertical features in (b) the conventional image shows 52% modulation (higher than the modulation in the anamorphic image), while the modulation on horizontal features is only 19%. A higher average intensity in the lines and spaces found in the anamorphic image indicates a higher background level. More scattered light from the bright-field target reaching the CCD at the lower angular separation (6 deg CRA) in the anamorphic image is a possible source of increased background and consequently decreased modulation compared to the vertical lines in the conventional image at 8 deg CRA. An increased background is also found in the large absorber feature (the number five) in the anamorphic image from Fig. 8.

The SHARP images, shown in Fig. 9, are taken from a through-focus series recorded by varying the object distance

Downloaded From: http://nanolithography.spiedigitallibrary.org/ on 07/15/2016 Terms of Use: http://spiedigitallibrary.org/ss/TermsOfUse.aspx

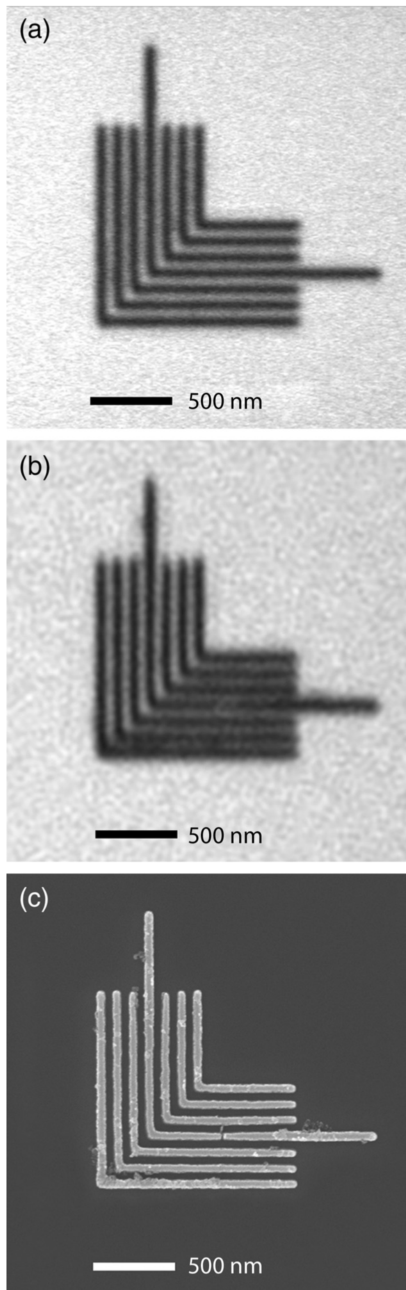

Fig. 9 SHARP aerial images of 50-nm CD elbows (mask scale), comparing (a) anamorphic imaging at 0.55 $4\times/8\times$ NA (6 deg CRA) with (b) conventional imaging at 0.5 $4\times$ NA (8 deg CRA), and (c) SEM-image of the $4\times$ elbow on the target.

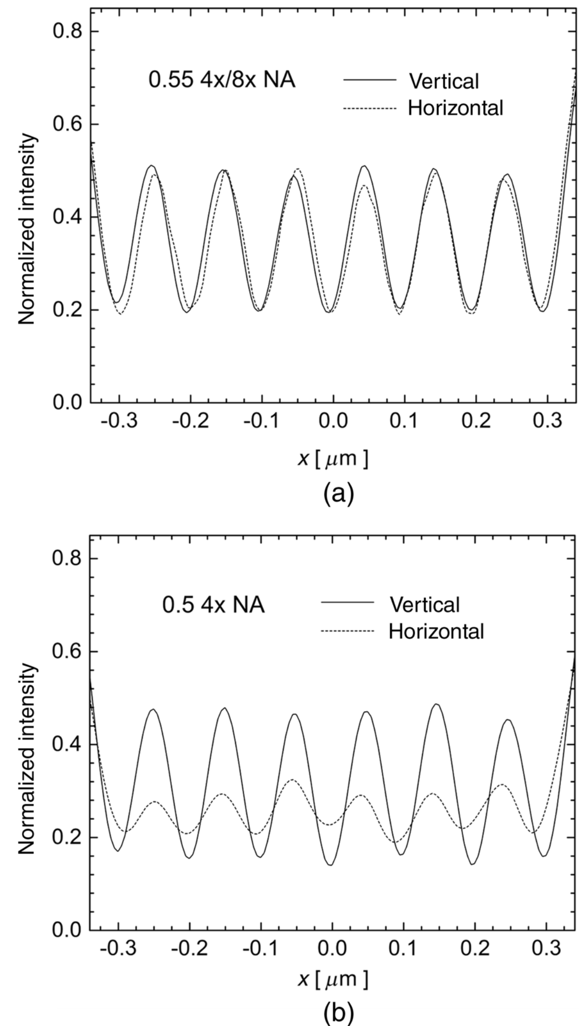

Fig. 10 Cross-section of the horizontal and vertical features of the 50-nm mask CD elbows from Fig. 9, comparing (a) anamorphic imaging at 0.55 $4\times/8\times$ NA (6 deg CRA) with (b) conventional imaging at 0.5 $4\times$ NA ($8\times$ CRA).

in 300-nm steps. Figure 11 shows plots of the modulation in the elbows through-focus, comparing (a) anamorphic and (b) conventional imaging. The evolution of the images through-focus is shown in Fig. 12. Aside from the overall lower modulation on horizontal features, the conventional series shows the same through-focus characteristics in the x- and y-directions. On vertical features, the modulation through-focus in the anamorphic data compares well to the characteristics of the conventional series. For horizontal features, the modulation curve of the anamorphic data is almost flat within a range of 2.4 μm. The depth of field exceeds the focal range of ± 1.2 μm covered in the series.

In EUV scanners, the depth of focus (on the wafer side) is the primary concern. Since the exit pupil is circular, depth of focus is expected to be uniform in an anamorphic scanner. It is smaller than the depth of field by a ratio of the demagnification squared (i.e., a factor of 16 for an isomorphic $4\times$ system). Accordingly, in an anamorphic $4\times/8\times$ system, the depth of field (on the mask side) is expected to be 16 times larger for vertical features and 64 times larger for horizontal features.

SHARP image data captures the mask-side through-focus behavior of an anamorphic system. As in isomorphic mode, for horizontal and vertical features, depth of focus (on the wafer side) can be calculated from the measured, mask-side depth of field by applying the corresponding factors. For two-dimensional patterns, the depth of focus on the wafer side is not simply obtained from SHARP image data. Further research is required to address this.

4 Summary

SHARP is an actinic EUV mask-imaging microscope targeted at a wide range of applications in EUV photomask

Downloaded From: http://nanolithography.spiedigitallibrary.org/ on 07/15/2016 Terms of Use: http://spiedigitallibrary.org/ss/TermsOfUse.aspx

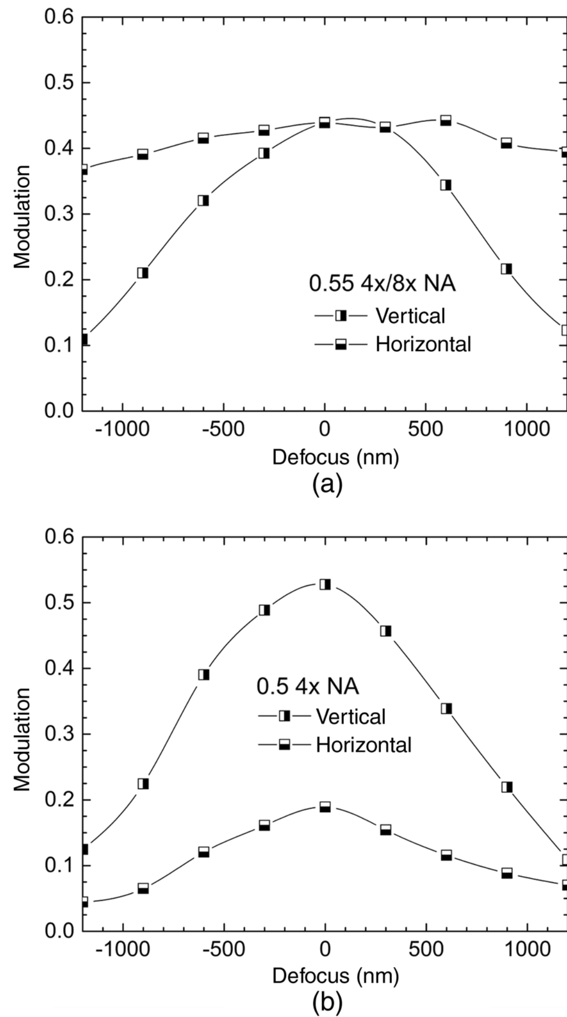

Fig. 11 Modulation of horizontal and vertical features through-focus in the (a) anamorphic and (b) conventional series of SHARP images, shown in Fig. 12.

research and development. The tool is designed to emulate imaging in EUV lithography scanners. The generation of EUVL succeeding the 0.33 NA systems will likely employ anamorphic imaging with different horizontal and vertical demagnification. SHARP is upgraded to emulate scanners with anamorphic projection optics.

Zoneplate lenses with an anamorphic $4\times/8\times$ NA of 0.55 are fabricated and installed in the tool. SHARP's Fourier synthesis illuminator readily produces source angular spectra matched to anamorphic imaging. Anamorphic test patterns down to 50-nm mask CD dense features are written on a multilayer-coated silicon wafer using 40 nm of nickel as the absorber material.

Test patterns are imaged in a demonstration experiment, comparing anamorphic imaging at 0.55 $4\times/8\times$ NA and 6 deg CRA to conventional imaging at 0.5 $4\times$ NA and 8 deg CRA. While the anamorphic images show the same image quality in the horizontal and vertical directions, conventional imaging suffers from a significant horizontal feature contrast loss that can be attributed to the limited angular bandwidth of the multilayer coating and shadowing from absorber features. The mask-side through-focus behavior

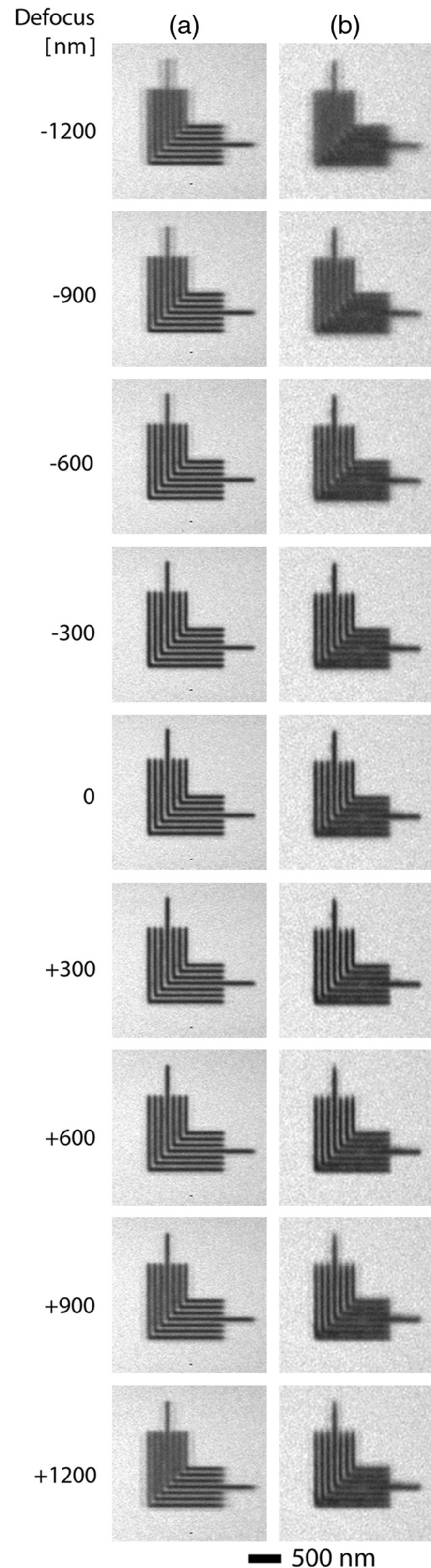

Fig. 12 Through-focus series of SHARP images, comparing through-focus behavior in (a) anamorphic imaging at 0.55 $4\times/8\times$ NA (6 deg CRA) with (b) conventional imaging at 0.5 $4\times$ NA (8 deg CRA).

of anamorphic and conventional EUV-imaging systems is discussed. SHARP image data captures the mask-side through-focus behavior of an anamorphic system. The factor two difference between the vertical and horizontal mask-side

Downloaded From: http://nanolithography.spiedigitallibrary.org/ on 07/15/2016 Terms of Use: http://spiedigitallibrary.org/ss/TermsOfUse.aspx

NA causes the depth of field to be four times larger for horizontal features than for vertical features.

The SHARP microscope provides a versatile platform for research related to anamorphic imaging in EUV lithography today. The consideration of various demagnifications, pupil aspect ratios, and illumination patterns can be used to guide progress in this area without the extensive modifications that all-reflective actinic mask-imaging microscopes could require.

References

1. M. Burkhardt and A. Raghunathan, "Best focus shift mechanism for thick masks," *Proc. SPIE* **9422**, 94220X (2015).
2. E. R. Hosler et al., "EUV and optical lithographic pattern shift at the 5 nm node," *Proc. SPIE* **9776**, 977616 (2016).
3. J. T. Neumann et al., "Mask effects for high-NA EUV: impact of NA, chief-ray-angle, and reduction ratio," *Proc. SPIE* **8679**, 867915 (2013).
4. J. van Schoot et al., "EUV lithography scanner for sub 8 nm resolution," *Proc. SPIE* **9422**, 94221F (2015).
5. B. Kneer et al., "EUV lithography optics for sub 9 nm resolution," *Proc. SPIE* **9422**, 94221G (2015).
6. T. Heil et al., "Anamorphic high NA optics enabling EUV lithography with sub 8 nm resolution," in *2015 Int. Sym. of Extreme Ultra Violet Lithography* (2015).
7. E. Gallagher et al., "Learning from native defects on EUV mask blanks," *Proc. SPIE* **9256**, 92560K (2014).
8. Y.-G. Wang et al., "Enhancing defect detection with Zernike phase contrast in EUV multilayer blank inspection," *Proc. SPIE* **9422**, 94221C (2015).
9. M. Lawliss et al., "Repairing native defects on EUV mask blanks," *Proc. SPIE* **9235**, 923516 (2014).
10. P.-Y. Yan et al., "Understanding EUV mask blank surface roughness induced LWR and associated roughness requirement," *Proc. SPIE* **9422**, 94220J (2015).
11. S. Raghunathan et al., "Experimental measurements of telecentricity errors in high-numerical-aperture extreme ultraviolet mask images," *J. Vac. Sci. Technol. B* **32**, 06F801 (2014).
12. V. Philipsen et al., "Imaging impact of multilayer tuning in EUV masks, experimental validation," *Proc. SPIE* **9235**, 92350J (2014).
13. K. A. Goldberg et al., "Actinic mask imaging: recent results and future directions from the SHARP EUV microscope," *Proc. SPIE* **9048**, 90480Y (2014).
14. K. A. Goldberg et al., "EUV actinic brightfield mask microscopy for predicting printed defect images," *Proc. SPIE* **9635**, 963514 (2015).
15. M. Benk et al., "Demonstration of 22-nm half pitch resolution on the SHARP EUV microscope," *J. Vac. Sci. Technol. B* **33**, 06FE01 (2015).
16. P. P. Naulleau et al., "Fourier-synthesis custom- coherence illuminator for extreme ultraviolet microfield lithography," *Appl. Opt.* **42**(5), 820–826 (2003).

Markus P. Benk is the project scientist at the SHARP microscope, Center of X-ray Optics, Lawrence Berkeley National Laboratory. He received his diploma in photo engineering from the Cologne University of Applied Sciences in 2006 and his PhD from RWTH Aachen University in 2011. His current research interests include sources, metrology and optics for soft x-rays, and extreme ultraviolet light.

Antoine Wojdyla is a postdoctoral fellow at the Lawrence Berkeley National Laboratory's Center for X-Ray Optics. He received his PhD from École Polytechnique in 2011, where he studied time-domain phase imaging in the far infrared range. His research interests include optical instrumentation and computational analysis of image data.

Weilun Chao leads the nanofabrication group of the Center for X-ray Optics. He received his PhD in electrical engineering from the University of California, Berkeley, in 2005. He specializes in electron-beam-based lithographic processes for dense nanostructures and EUV/x-ray diffractive optics. Current research interests include complex diffractive optics, 3-D nanostructures, and nanodevices for life science.

Farhad Salmassi has been with the Center for X-Ray Optics at Lawrence Berkeley National Laboratory since 1998. He received his BS degree in applied mathematics from San Francisco State University and has been involved with thin films and nanofabrication for over 16 years. He runs the multilayer deposition laboratory and has contributed to the Extreme Ultraviolet Lithography program and other x-ray related work, with over 70 publications in professional and refereed journals.

Sharon Oh is a postdoctoral fellow at the Center for X-Ray Optics, Lawrence Berkeley National Laboratory. She received her BS degree in engineering physics and MS degree in applied science and technology from the University of California, Berkeley, and her PhD in mechanical engineering from National University of Singapore in 2014. She specializes in the areas of micro- and nanofabrication and is currently engaged in the development and nanofabrication of x-ray diffractive optics.

Yow-Gwo Wang is a PhD candidate at Department of Electrical Engineering and Computer Sciences, University of California at Berkeley and also a graduate student researcher at Center for X-ray Optics, Lawrence Berkeley National Laboratory, under the guidance of Prof. Andy Neureuther and Dr. Patrick Naulleau. He received the SPIE BACUS Photomask Scholarship in 2015. His research is focusing on design, fabrication, and testing of mask/lens concept for EUV aerial image monitoring and inspection.

Ryan H. Miyakawa is an EUV project scientist at the Center for X-ray Optics at Lawrence Berkeley National Lab, where he works with the SEMATECH Berkeley MET performing EUV imaging, interferometry, and lithography.

Patrick P. Naulleau received his BS and MS degrees in electrical engineering from Rochester Institute of Technology, Rochester, New York, and his PhD in electrical engineering from the University of Michigan, Ann Arbor, in 1997. He joined the Berkeley Lab working in EUV lithography and metrology. In April 2010, he became director of the Center for X-ray Optics at the Berkeley Lab. He has over 300 publications and 19 patents and is a fellow of OSA and SPIE.

Kenneth A. Goldberg is the optics group leader for the Advanced Light Source at Lawrence Berkeley National Laboratory, where he specializes in the development of EUV and soft x-ray technologies, including lithography, mask imaging, and interferometry. Recently, he led the development of the SHARP EUV mask-imaging microscope. He holds an AB degree in physics and applied math, and a PhD in physics from the University of California, Berkeley.

Downloaded From: http://nanolithography.spiedigitallibrary.org/ on 07/15/2016 Terms of Use: http://spiedigitallibrary.org/ss/TermsOfUse.aspx